How galaxies trace large scale structure at $z \sim 3$?

Anna Durkalec[1], Olivier Le Fèvre[2],
Agnieszka Pollo[1,3] and the VUDS Collaboration

1. National Centre for Nuclear Research; Andrzeja Soltana 7, 05-400 Otwock, Poland
2. Aix Marseille Université, CNRS, LAM (Laboratoire d'Astrophysique de Marseille) UMR 7326, 13388, Marseille, France
3. Astronomical Observatory of the Jagiellonian University, Orla 171, 30-001 Cracow, Poland

We study the dependence of galaxy clustering on luminosity and stellar mass in the redshift range $2 < z < 3.5$ based on spectroscopic data from the VIMOS Ultra Deep Survey (VUDS). In our work, by applying halo occupation distribution (HOD) models to the correlation function measurements for different galaxy samples, we showed how dark matter halo mass and large scale bias depend on luminosity and stellar mass of galaxies and how this dependence changes with redshift. Additionally, we measured the stellar-to-halo mass ratio (SHMR) and found a significant model-observation discrepancy for low-mass galaxies at $z \sim 3$, suggesting a higher than expected star formation efficiency of these galaxies.

1 Introduction

In the paradigm of ΛCDM cosmology galaxies form and evolve inside overdense regions of the dark matter (DM; see White & Rees, 1978). In this scenario, both galaxies (in general luminous mater) and underlying dark matter create the large scale structure of the universe - a web-like network of clusters, superclusters and larger structures. Its evolution is driven mostly by the dominant dark matter component, for which methods of direct observations are currently very limited. In order to study changes of large scale structure, we need to rely only on the observations of its visible baryonic component, which is connected to the dark matter distribution. However, this luminous-dark matter relation (called galaxy *bias*) is not straightforward due to the physics of the baryonic mater not applying to dark matter. I.e., star formation, supernova feedback and galaxy merging (e.g., Kaiser, 1984; Bardeen et al., 1986; Mo & White, 1996; Kauffmann et al., 1997). These effects naturally have impact on observed properties of galaxies. Therefore studies of the dependence of galaxy bias on various galaxy properties such as luminosity, stellar mass, or colour, proved to be crucial in order to understand the history of structure formation. This is especially true for higher redshift ranges ($z > 2$), for which these relations have been difficult to establish because of the limited data availability.

With this aim in mind, we study the dependence of galaxy clustering on their luminosity and stellar mass in the redshift range $2 < z < 3.5$ using spectroscopic data from the VIMOS Ultra Deep Survey (VUDS, Le Fèvre et al., 2015). In our work we make use of the measurements of two-point correlation function quantified using both a power-law approximation and the five parameter HOD (Halo Occupation Distribution) model. Consequently, we are able to estimate the characteristic halo masses, galaxy bias, satellite fraction and stellar-to-halo mass ratio (SHMR) for population of bright UV galaxies. We discuss our results in terms of large scale structure properties and evolution from redshift $z \sim 3$ to present times.

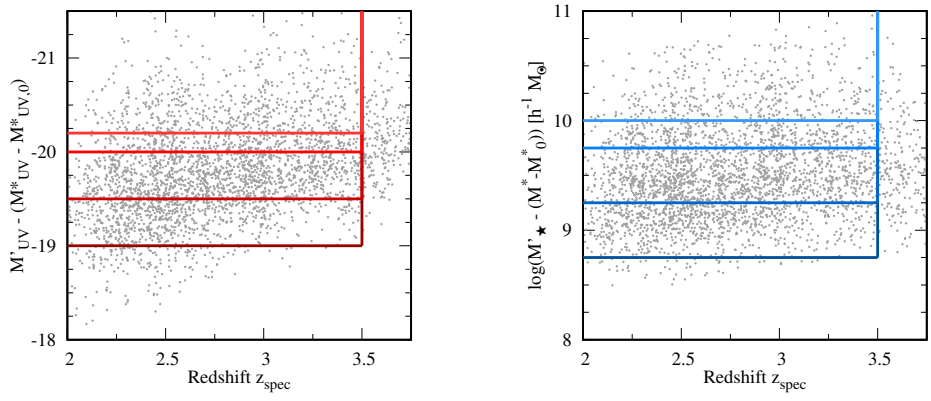

Fig. 1: Construction of the volume-limited galaxy subsamples with different luminosities (left panel) and stellar masses (right panel). In each figure black dots represent the distribution of VUDS galaxies as a function of spectroscopic redshift.

2 Data sample

Our galaxy sample contains a total number of 3236 objects with reliable spectroscopic redshifts in the range $2 < z < 3.5$ selected from VUDS (Le Fèvre et al., 2015). The sample consists of galaxies observed in three independent fields, COSMOS, VVDS-02h, and ECDFS covering a total area of 0.92 deg^2. We divided these galaxies into four volume-limited luminosity subsamples, with the selection cuts made in the UV rest-frame absolute magnitudes, and four stellar mass subsamples. The distributions of VUDS galaxies as a function of spectroscopic redshift and applied selection cuts are presented in Fig. 1. The UV absolute magnitudes and stellar masses have been normalized, at each redshift, to the corresponding characteristic quantities (namely Schechter parameters M_*, see Schechter, 1976) to correct for the mean brightening (mass increase) of galaxies due to their evolution and to ease the comparison between subsamples. Each sample have been chosen to contain a sufficient number of galaxies for a reliable correlation function measurement (see Durkalec et al., 2018, for details).

3 Methods

We measured the two-point real-space correlation function $\xi(r_\mathrm{p}, \pi)$ using the Landy-Szalay estimator (Landy & Szalay, 1993), which we then integrate over the line of sight to obtain two-point projected correlation function free from the redshift-space distortions (Davis & Peebles, 1983):

$$w_\mathrm{p}(r_\mathrm{p}) = 2 \int_0^\infty \xi(r_\mathrm{p}, \pi) d\pi. \tag{1}$$

The technical details of this measurements, such as methods of obtaining π_max - upper limit of integration, corrections applied in order to account for various systematics originating in the VUDS survey properties are described in Durkalec et al. (2015). In particular, since in our study we are using the data sample divided unequally be-

tween three independent fields, we use the appropriate weighting scheme. During measurements of $\xi(r_\mathrm{p}, \pi)$, each pair (galaxy-galaxy, galaxy-random, and random-random) is multiplied by the number of galaxies in this field per unit volume. Errors of correlation function are obtained using blockwise bootstrap resampling method.

To quantify the measurements of correlation function, we apply commonly used, five-parameter halo occupation distribution models (HOD, see e.g., Zheng et al., 2005, 2007; Zehavi et al., 2011). In the HOD framework a number of galaxies that occupy a typical DM halo $\langle N_\mathrm{g}\,(M_\mathrm{h})\rangle$ depends on the halo mass M_h and is given as a sum of the mean halo occupation functions of the central $\langle N_\mathrm{cen}\,(M_\mathrm{h})\rangle$ and satellite $\langle N_\mathrm{sat}\,(M_\mathrm{h})\rangle$ galaxies:

$$\langle N_\mathrm{cen}\,(M_\mathrm{h})\rangle = \frac{1}{2}\left[1 + \mathrm{erf}\left(\frac{\log M_\mathrm{h} - \log M_\mathrm{min}}{\sigma_{\log M}}\right)\right] \tag{2}$$

$$\langle N_\mathrm{sat}\,(M_\mathrm{h})\rangle = \langle N_\mathrm{cen}\,(M_\mathrm{h})\rangle \times \left(\frac{M_\mathrm{h} - M_0}{M_1}\right)^\alpha. \tag{3}$$

Where erf stands for an "error function" in a form $\mathrm{erf}(z) = \frac{2}{\sqrt{\pi}}\int_0^z e^{-t^2}dt$. The model contains five free parameters: M_min - the minimal halo mass for which a half of the DM haloes host one galaxy (with luminosity/stellar mass above the threshold limit), M_1 - the DM halo mass for which on average halo contains one central and one additional satellite galaxy, M_0 - the cut-off mass scale, $\sigma_{\log M}$ - related to the scatter between the galaxy luminosity (or stellar mass) and halo mass, and α - power-law slope of the satellite mean occupation function. Using best-fitting HOD parameters we can derive additional quantities describing DM haloes and galaxy population properties, such as an average host halo mass $\langle M_\mathrm{h}\rangle$, large scale galaxy bias b_g and satellite fraction f_s.

4 Results and discussion

The main conclusion of our study is that at redshift $z \sim 3$ there is a clear luminosity and stellar mass dependence of galaxy clustering; the brightest and the most massive galaxies are more strongly clustered than their less luminous and less massive counterparts. These observations are in agreement with the lower redshift studies (e.g., Zheng et al., 2007; Abbas et al., 2010; Zehavi et al., 2011) and overall with the predictions of the hierarchical scenario of structure formation. In this scenario, the mass overdensities of the density field collapsed overcoming the cosmological expansion. The initially stronger, and more massive, overdensities grew faster, hence their stronger clustering pattern imprinted in the dark matter density field. With time, the resulting dark matter haloes merged together, forming larger haloes, which served as the environment in which galaxies formed and evolved later on (Press & Schechter, 1974; White, 1976). The strongest and most clustered overdensities produced the largest haloes, containing the corresponding amount of baryons, which - in turn - agglomerated to produce the largest and most massive (consequently also the most luminous) galaxies.

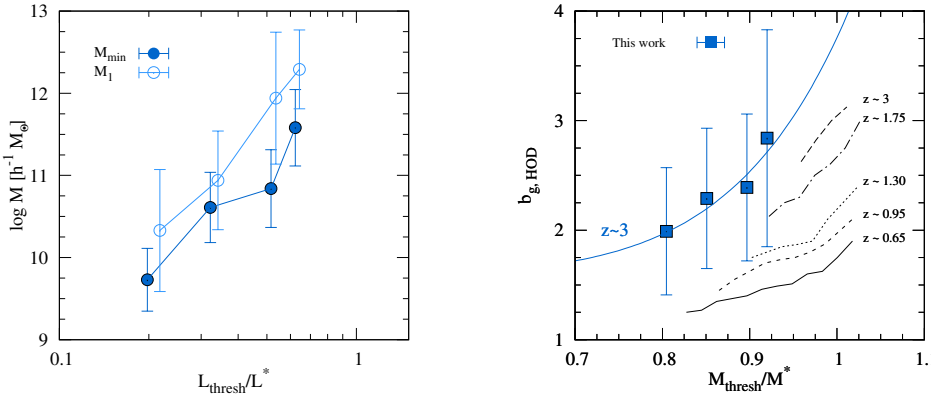

Fig. 2: Left panel: Best-fit HOD characteristic DM halo masses $M_{\rm min}$ and M_1 at $z \sim 3$ hosting galaxies with UV absolute magnitudes above a given luminosity threshold. Right panel: Large scale galaxy bias $b_{\rm g,HOD}$ obtained using best-fit HOD parameters, as a function of stellar mass of galaxy population. Filled points represent results from this study at $z \sim 3$ and are compared with lower-redshift measurements by McCracken et al. (2015).

4.1 DM halo masses of galaxies with different properties

In terms of the HOD parameters, we observe an increase in the characteristic DM halo mass hosting galaxies with rising luminosity and stellar mass. As an example, in the left panel of Fig. 2, we present these changes for the luminosity selected subsamples (for full discussion see Durkalec et al., 2018). The minimum halo mass $M_{\rm min}$ increases from $M_{\rm min} = 10^{9.73\pm0.51}$ h^{-1} M$_\odot$ to $M_{\rm min} = 10^{11.58\pm0.62}$ h^{-1} M$_\odot$ for galaxies with the median UV absolute magnitude $M_{\rm UV}^{\rm med} = -19.84$ and $M_{\rm UV}^{\rm med} = -20.56$, respectively. At the same time, for galaxy subsamples selected according to stellar mass, $M_{\rm min}$ grows from $M_{\rm min} = 10^{9.75\pm0.48}$ h^{-1} M$_\odot$ to $M_{\rm min} = 10^{11.23\pm0.56}$ h^{-1} M$_\odot$ for galaxies with $\log M_\star^{\rm med} = 9.48$ h^{-1} M$_\odot$ to $\log M_\star^{\rm med} = 10.24$ h^{-1} M$_\odot$. We also observe a substantial growth in the satellite halo mass M_1 with increasing luminosity and stellar mass of galaxies. The M_1 increases from $M_1 = 10^{10.33\pm0.74}$ h^{-1} M$_\odot$ for the faintest galaxy subsample to $M_1 = 10^{12.29\pm0.48}$ h-1 M$_\odot$ for the most luminous galaxies. Similarly, for the stellar mass selected subsamples: M_1 increases from $M_1 = 10^{10.21\pm0.69}$ h^{-1} M$_\odot$ to $M_1 = 10^{11.57\pm0.65}$ h^{-1} M$_\odot$ from the less to the most massive galaxy subsamples, respectively.

4.2 Large scale galaxy bias

As shown in the right panel of Fig. 2, measurements of the large scale galaxy bias indicate that it is (1) significantly higher than in the local universe, which means that in the early stages of evolution galaxies were highly biased tracers of the underlying dark matter density field, and (2) galaxy bias is stellar mass dependent (also luminosity dependent as described in details in Durkalec et al., 2018). The latter observation is in good agreement with the previous low-redshift studies (e.g., Norberg et al., 2002; Tegmark et al., 2004; Meneux et al., 2008; Zehavi et al., 2011;

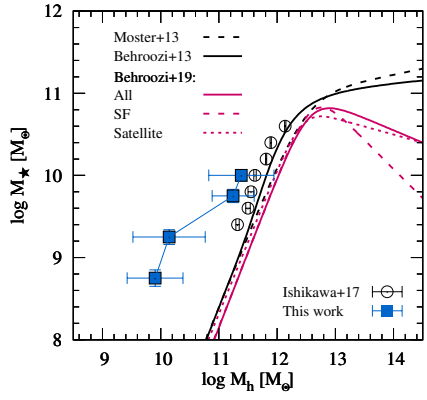

Fig. 3: Stellar to halo mas ratio of central galaxies with different stellar masses at $z \sim 3$ (blue squares). Our measurements are compared with the similar results obtained for LBGs galaxies by Ishikawa et al. (2017) at the same redshift (open circles). Various lines represent theoretical models of SHMR by Behroozi et al. (2013, 2019); Moster et al. (2013) as labeled. From Behroozi et al. (2019) we show theoretical predictions for all galaxies (solid line), star forming galaxies (dashed line), and satellite galaxies (dotted line).

Mostek et al., 2013) and with the expectation of the hierarchical model of the large scale structure formation.

4.3 Stellar-to-halo mass relation for low mass galaxies at $z \sim 3$

Finally, we focus on the relation between DM halo and stellar mass for each galaxy sample - so-called stellar to halo mas ratio (SHMR). The comparison between our results and the $z = 3$ theoretical model predictions by Behroozi et al. (2013, 2019) and Moster et al. (2013) show a significant discrepancy for low-mass ($M_\star < 10^{9.25}$ $M_\odot$) galaxies, indicating a higher than expected star formation occurring in these galaxies. A possible explanation are the various positive feedback effects, such as supernovae explosions or presence of Active Galactic Nucleus (AGN), influencing these low-mass (small) galaxies, and stimulating more effective star formation similarly as it is observed for the dwarf galaxies in the local universe (see e.g., Kawata et al., 2014; Oñorbe et al., 2015; Chen et al., 2016; Papastergis & Shankar, 2016). However, the other possible explanation lies in the flaws of techniques used in the presented theoretical models to infer SHMR. Behroozi et al. (2013) note that the low-mass end of the theoretical model is a power-law extrapolation of the results based on the measurements for massive galaxies. This simple method might not be enough and accurate high redshift observations are needed to constrain the model. Our results are, therefore, one of the first to bring us closer toward this goal.

Acknowledgements. AD is supported by the Polish National Science Centre grant UMO-2015/17/D/ST9/02121. AP is suported by the NCN grant UMO-2018/30/M/ST9/00757 and MNiSW grant DIR/WK/2018/12. This work is based on data products made available at the CESAM data centre, Laboratoire d'Astrophysique de Marseille. This work partly uses observations obtained with MegaPrime/MegaCam, a joint project of CFHT

and CEA/DAPNIA, at the Canada-France-Hawaii Telescope (CFHT) which is operated by the National Research Council (NRC) of Canada, the Institut National des Sciences de l'Univers of the Centre National de la Recherche Scientifique (CNRS) of France, and the University of Hawaii.

References

Abbas, U., et al., *MNRAS* **406**, 1306 (2010)

Bardeen, J. M., Bond, J. R., Kaiser, N., Szalay, A. S., *ApJ* **304**, 15 (1986)

Behroozi, P., Wechsler, R. H., Hearin, A. P., Conroy, C., *MNRAS* **488**, 3, 3143 (2019)

Behroozi, P. S., Wechsler, R. H., Conroy, C., *ApJ* **770**, 57 (2013)

Chen, J., Bryan, G. L., Salem, M., *MNRAS* **460**, 3335 (2016)

Davis, M., Peebles, P. J. E., *ApJ* **267**, 465 (1983)

Durkalec, A., et al., *A&A* **583**, A128 (2015)

Durkalec, A., et al., *A&A* **612**, A42 (2018)

Ishikawa, S., et al., *ApJ* **841**, 8 (2017)

Kaiser, N., *ApJ* **284**, L9 (1984)

Kauffmann, G., Nusser, A., Steinmetz, M., *MNRAS* **286**, 795 (1997)

Kawata, D., et al., *MNRAS* **438**, 1208 (2014)

Landy, S. D., Szalay, A. S., *ApJ* **412**, 64 (1993)

Le Fèvre, O., et al., *A&A* **576**, A79 (2015)

McCracken, H. J., et al., *MNRAS* **449**, 901 (2015)

Meneux, B., et al., *A&A* **478**, 299 (2008)

Mo, H. J., White, S. D. M., *MNRAS* **282**, 347 (1996)

Mostek, N., et al., *ApJ* **767**, 89 (2013)

Moster, B. P., Naab, T., White, S. D. M., *MNRAS* **428**, 3121 (2013)

Norberg, P., et al., *MNRAS* **332**, 827 (2002)

Oñorbe, J., et al., *MNRAS* **454**, 2092 (2015)

Papastergis, E., Shankar, F., *A&A* **591**, A58 (2016)

Press, W. H., Schechter, P., *ApJ* **187**, 425 (1974)

Schechter, P., *ApJ* **203**, 297 (1976)

Tegmark, M., et al., *ApJ* **606**, 702 (2004)

White, S. D. M., *MNRAS* **177**, 717 (1976)

White, S. D. M., Rees, M. J., *MNRAS* **183**, 341 (1978)

Zehavi, I., et al., *ApJ* **736**, 59 (2011)

Zheng, Z., Coil, A. L., Zehavi, I., *ApJ* **667**, 760 (2007)

Zheng, Z., et al., *ApJ* **633**, 791 (2005)